X-ray Spectroscopy of Nitrile Hydratase at pH 7 and 9[†]

Robert C. Scarrow,*[,‡] Bridget A. Brennan,[§] John G. Cummings,[§] Haiyong Jin,[§] Daihung J. Duong,[‡] James T. Kindt,[‡] and Mark J. Nelson[§]

Department of Chemistry, Haverford College, Haverford, Pennsylvania 19041-1392, and Central Research and Development, E. I. du Pont de Nemours & Company, Wilmington, Delaware 19880-0328

Received January 23, 1996; Revised Manuscript Received April 23, 1996[⊗]

ABSTRACT: The iron K-edge X-ray absorption spectrum of *Rhodococcus* sp. R312 (formerly *Brevibacterium* sp. R312) nitrile hydratase in frozen solutions at pH 7 and 9 has been analyzed to determine details of the iron coordination. EXAFS analysis implies two or three sulfur ligands per iron and overall six coordination; together with previous EPR and ENDOR results, this implies an N_3S_2O ligation sphere. The bond lengths from EXAFS analysis [r_{av}(Fe−S) = 2.21 Å at pH 7.3; r_{av}(Fe−N/O) = 1.99 Å] support *cis* coordination of two cysteine ligands and conclusively rule out nitric oxide coordination to the iron, a possibility proposed on the basis of an FTIR difference experiment [Noguchi, T., Honda, J., Nagamune, T., Sasabe, H., Inoue, Y., & Endo, I. (1995) *FEBS Lett. 358,* 9−12]. The higher-frequency EXAFS can be simulated well by inclusion of multiple scattering from two or three imidazole ligands; the fit to the data is improved if first-sphere multiple scattering pathways are also included. A slight shortening (by 0.02 ± 0.01 Å) of one or both Fe−S bonds when the pH is raised from 7.3 to 9.0 is consistent with shifts observed in the Raman spectrum [Brennan et al. (1996) *Biochemistry 35,* 10068−10077].

Nitrile hydratases are bacterial enzymes that catalyze the partial hydration of nitriles to give amides. They are of interest because of their use in commercial-scale synthesis of amides (Kobayashi et al., 1992). Although the reaction catalyzed formally involves no oxidation or reduction, nitrile hydratases contain the redox-active metals iron or cobalt in a non-heme, trivalent, low-spin state (Sugiura et al., 1987; Nagasawa et al., 1988; R. C. Scarrow and M. J. Nelson, unpublished).

We have been studying the iron-containing nitrile hydratase from an amidase-deficient mutant of *Rhodococcus* sp. R312, formerly *Brevibacterium* sp. R312 (Briand et al., 1994). The iron-containing nitrile hydratases are the first examples of non-heme low-spin centers in proteins. The identity of the ligands has been inferred from a variety of spectroscopic studies employing nitrile hydratase from *Rhodococcus* sp. R312. A water or hydroxide ligand was inferred from EPR line broadening in spectra of samples prepared in $H_2{}^{17}O$ (Sugiura et al., 1987) and subsequently confirmed by electron nuclear double resonance (ENDOR)[1] spectroscopy (Jin et al., 1993). Three nitrogenous ligands, probably histidines, have been identified from ENDOR studies of ^{14}N and ^{15}N couplings to the electron spin (Jin et al., 1993). Thiolate coordination from cysteine has been inferred from X-ray absorption, UV/visible, and resonance Raman spectroscopy (Nelson et al., 1991; Brennan et al., 1996). Because the X-ray absorption spectroscopy (XAS) indicated the presence of at least two sulfur atoms bound to the iron, and because low-spin Fe^{3+} is virtually always six- (and never seven-) coordinate, the metal site was suggested to be $Fe^{3+}(Cys^-)_2(His)_3(OH_{1\ or\ 2})$.

Other groups have reported biochemical investigation of iron-containing nitrile hydratases from *Rhodococcus* sp. R312 (Nagasawa et al., 1986), *Rhodococcus* sp. N-771 (Nagamune et al., 1990), and *Pseudomonas chlororaphis* (Nagasawa et al., 1988), and the sequences of the genes encoding the enzymes from *Rhodococcus* sp N-774 [a close relative if not identical to *Rhodococcus* sp. R312 (Mayaux et al., 1990)], *Rhodococcus erythropolis* JCM6823, and *P. chlororaphis* have been reported (Ikehata et al., 1989; Duran et al., 1993; Nishiyama et al., 1991). These enzymes all appear to be $\alpha_2\beta_2$ tetramers. The amino acid sequences of the *Rhodococcus* sp. N774 and the *R. erythropolis* JCM6823 nitrile hydratases are approximately 95% identical, while those of the *Rhodococcus* sp. N-774 and *P. chlororaphis* are approximately 60% identical. The visible and EPR spectra associated with the metal centers in the active forms of the nitrile hydratases from *Rhodococcus* sp. R312, *Rhodococcus* sp. N-774, and *P. chlororaphis* are also virtually identical (Nagasawa et al., 1986, 1988; Sugiura et al., 1987; Nagamune

[†] X-ray data were collected at the National Synchrotron Light Source, Brookhaven National Laboratory, which is supported by the U.S. Department of Energy, Divisions of Materials Science and Chemical Science (DOE Contract DE-AC02-76CH00016). Research at Haverford College supported by the Undergraduate Biological Sciences Education Initiative of the Howard Hughes Medical Institute. Contribution 7319 from Central Research and Development.

* To whom correspondence should be addressed.

[‡] Haverford College.

[§] E. I. du Pont de Nemours & Company.

[⊗] Abstract published in *Advance ACS Abstracts,* July 15, 1996.

[1] Abbreviations: ADIT, anion of 5-amino-2,3-dimethyl-4-azahex-3-ene-2-thiol; BVS, bond valence sum; CSD, Cambridge Structure Database; dedtc, *N,N*-diethyldithiocarbamate; ENDOR, electron nuclear double resonance; EXAFS, extended X-ray absorption fine structure; FSMS, first-sphere multiple scattering; HEPES, *N*-(2-hydroxyethyl)-piperazine-*N*-2-ethanesulfonic acid; L_1, 1,4,7-tris(4′-*tert*-butyl-2′-mercaptobenzyl)-1,4,7-triazacyclononane; L_2, 1,4,7-tris(2′-mercaptopropyl)-1,4,7-triazacyclononane; Met, methionine; MTG, dianion of dimethylglyoxime *S*-methyldithiocarbazone; TIM, 2,3,9,10-tetramethyl-1,4,8,11-tetraazacyclotetradeca-1,3,8,10-tetrene; $T^{OMe}PP$, dianion of *meso*-tetrakis(4-methoxyphenyl)porphin; TPP, dianion of *meso*-tetraphenylporphin; tsa, 5-Cl-tsa, 5-Br-tsa, dianion of (substituted) salicylaldehyde thiosemicarbazone; XANES, X-ray absorption near-edge spectroscopy; XAS, X-ray absorption spectroscopy (includes EXAFS and XANES).

S0006-2960(96)00164-X CCC: $12.00

et al., 1990, 1992). Although there are differences in substrate specificity among these enzymes, it is very likely that the major features of protein structure and, in particular, the coordination of the iron are the same in the active forms of nitrile hydratases from all of these species. One significant difference, however, is that the nitrile hydratases from *Rhodococcus* sp. R312 and N-771 are expressed in an inactive form and require activation by light (Nagamune et al., 1990; M. J. Nelson, unpublished), whereas the enzyme from *P. chlororaphis* is synthesized in an active form (Nakajima et al., 1987).

We are continuing to develop XAS as a tool for the study of the chemical mechanism of nitrile hydration, as well as the physical mechanism of photoactivation of nitrile hydratase from *Rhodococcus* sp. R312. Our previous X-ray spectroscopic study (Nelson et al., 1991) was performed on solutions frozen at pH 7.8, which we now know contained a mixture of low- and high-pH forms (Brennan et al., 1996). To confirm that our earlier conclusions from XAS apply to both the low- and high-pH forms of nitrile hydratase, we have now determined the X-ray spectra of nitrile hydratase frozen at pH 7.3 (exclusively the low-pH form), pH 7.8, and pH 9.0 (where the high-pH form predominates). In the analysis of the spectra, we have looked for evidence regarding the relative orientation (*cis* or *trans*) of the two sulfur ligands as well as for the structural basis of the pH dependent changes in the visible, EPR, and resonance Raman spectra. In addition, a recent report of NO coordination to iron in nitrile hydratases (Noguchi et al., 1995) has prompted us to look for evidence in the EXAFS spectrum for or against Fe−NO bonds.

EXPERIMENTAL PROCEDURES

We have used the Cambridge Structure Database and the associated QUEST software to aid in modeling the geometry of the iron site in nitrile hydratase and in interpretation of the results (Allen et al., 1991). Bond valence sums are calculated as BVS $= \sum_i \exp[(r_o - r_i)/0.37$ Å], where the sum is over all Fe−X bonds with length r_i. We have used values of r_o derived for (high-spin) Fe^{3+} compounds: 1.759 Å for Fe−O bonds, 2.149 Å for Fe−S bonds (Brown & Altermatt, 1985), and 1.831 Å for Fe−N bonds (Scarrow et al., 1994).

XANES and EXAFS Spectroscopy. Nitrile hydratase was purified according to Brennan et al. (1996). The samples for XAS were prepared in either pH 7.3 100 mM HEPES, pH 7.8 10 mM HEPES, or pH 9.0 50 mM borate buffer, all with 40 mM sodium butyrate as a stabilizing agent (Nagasawa et al., 1986). The state of the iron center (low- or high-pH form) was verified by EPR before the XAS samples were prepared (Brennan et al., 1996). Samples were concentrated by ultrafiltration in Centricon units (Amicon). The concentrated samples were frozen in sample holders and maintained during data collection in an evacuated chamber at either 30 K using a Displex refrigeration unit (pH 7.3 and 9.0 samples) or 80 K using a liquid nitrogen-cooled cold finger (pH 7.8 samples).

Using previously described procedures (Scarrow et al., 1994), data were obtained at NSLS beam line X9a using a Si 111 monochromator and a 13-element Ge solid state detector (Canberra). In addition, one XANES spectrum was obtained at higher resolution at NSLS beam line X19a using a Si 220 monochromator.

Data Analysis. General procedures for analysis using the program *SSExafs* have been described previously (Scarrow et al., 1994). Definitions of χ (EXAFS), k (the photoelectron wavenumber), and r' (the apparent Fe−X distance in the Fourier transform of $k^3\chi$) are in accord with general usage (Scott, 1985). In least squares fitting, the residual minimized and reported is $\epsilon_\nu^2 = [n_{idp}/(n_{idp} - n_p)] \times$ average $[(y_{data} - y_{calc})/\sigma_{data}]^2$, where y is either $k^3\chi$ or its Fourier transform, n_p is the number of refined parameters, and σ_{data} is the estimated uncertainty of the data. For unfiltered refinements, n_{idp} is the number of data points; for fits to Fourier-transformed or filtered spectra, $n_{idp} = (2\Delta r'\Delta k)/\pi$, where Δk is the range of $k^3\chi$ transformed and $\Delta r'$ is the range of refinement or back-transform (Bunker et al., 1991). The uncertainty range of each refined parameter is determined as the range over which ϵ_ν^2 increases by no more than 1.0 above its minimum value when other parameters are allowed to refine; this relatively conservative method of error estimation follows the recommendations of the International Workshops on Standards and Criteria in XAFS (Bunker et al., 1991).

Baseline fitting and determination of the edge height was accomplished by fitting data from 6980 to 7900 eV, except for data from 7124 to 7144 eV (immediately above the edge, a region which is difficult to successfully simulate). A cubic-spline baseline (spline points at 7125, 7405, and 7645 eV) was fit simultaneously with edge and EXAFS parameters. For these initial fits, $\sigma_{data} = 0.001$ for $E < E_0 = 7125$ eV and 1.0 $Å^{-3}/k^3$ for data above the edge (equivalent to fitting $k^3\chi$ with $\sigma_{data} = 1.0$ $Å^{-3}$). The edge was modeled as an integral of a 75% Gaussian + 25% Lorentzian peak (Scarrow et al., 1994), and the overlapping pre-edge peaks were assumed to be Gaussian with a common width.

Simulation of First-Sphere EXAFS. Shells of sulfur and nitrogen scatterers were modeled using amplitude and phase functions derived from FEFF 5 (Rehr et al., 1991; Rehr et al., 1992). The refined $\Delta\sigma^2$ parameter indicates additional thermal or positional disorder beyond that calculated by FEFF using a Debye temperature of 700 ($\sigma^2 = 0.0047$ Å^2 for Fe−N distances of 2.0 Å; $\sigma^2 = 0.0026$ Å^2 for Fe−S distances of 2.2 Å). The construction of the functions for sulfur scatterers was similar to that described for nitrogen (Scarrow et al., 1994); coordinates of $[Fe_4S_4(SC_6H_5)_4]^{2-}$ (Que et al., 1974) were used for calculating atom potentials. An amplitude multiplication factor of 0.75 and an E_0 of 7122 eV was used with the Fe−S scattering functions so that EXAFS fits of crystallographically characterized model complexes [Fe(dedtc)$_3$, for instance] give approximately correct n_S and r_{Fe-S} values. The need for the amplitude reduction factor of approximately 0.75 has been verified in a study of the iron−sulfur cluster of nitrogenase iron protein (Seefeldt et al., 1996). No amplitude reduction and $E_0 =$ 7125 eV were used with Fe−N functions (Scarrow et al., 1994).

Fits to unfiltered ("raw") $k^3\chi$ are for 2.2 $Å^{-1} < k <$ 14.3 $Å^{-1}$; $\sigma_{data} = 0.5$ $Å^{-3}$ to account for the outer-sphere EXAFS and noise. The first-sphere Fourier-filtered EXAFS refers to $k^3\chi$ Fourier-transformed over the range $k = 1.0-14.3$ $Å^{-1}$ and back-transformed from $r' = 1.0-2.3$ Å (no windowing). The Fourier-filtered EXAFS between $k = 2.2$ and 14.3 $Å^{-1}$ was fit ($n_{idp} = 10.1$) using σ_{data} linearly interpolated from (k, σ_{data}) = (2.2, 0.14), (4, 0.19), (8, 0.26), (10, 0.42), (13, 0.88), and (14.3 $Å^{-1}$, 0.56 $Å^{-3}$) (Scarrow et al., 1994).

Simulation of the Outer-Sphere EXAFS. FEFF can calculate the EXAFS for both single and multiple scattering paths and was used to simulate the Fourier transform of $k^3\chi$ in its outer-sphere region ($r' > 2.3$ Å). Initial simulations indicated that, because of larger calculated disorder parameters for the outer sphere and multiple scattering paths, the $k^3\chi$ due to these paths becomes less than the noise level of the data at about $k = 10$ Å^{-1}. Therefore, we report fits in which $k^3\chi$ from $k = 2$ to 10 Å^{-1} is Fourier-transformed; parameters from these fits are not significantly different from those for fits where the $k^3\chi$ from $k = 1$ to 14.3 Å^{-1} are fit. We also compared results from fits to just the outer-sphere region of the FT (2.3 Å $< r' <$ 4.2 Å) and those to the combined first- and outer-sphere regions (multisphere fits; 1.0 Å $< r' <$ 4.2 Å) and find that the two approaches give refined parameters well within uncertainty of each other. The parameter uncertainties are smaller (particularly for the refined bond lengths r_N and r_S) in the multisphere fits, and thus, we report results from these fits in this paper. The rms magnitude of the Fourier transform of the pH 7.3 spectrum between $r' = 5$ and 10 Å is 0.2 Å^{-3}; this value was used for σ_{data}.

For the outer-sphere EXAFS calculations, imidazole groups were given fixed planar geometry from bond lengths and angles for 61 Fe−Im units found in a search of the Cambridge Structural Database. Bond distances (in angstroms) were fixed as follows (N_1 is bound to Fe; ranges in parentheses are as found in the Database): N_1-C_2, 1.31 (1.27−1.35); N_1-C_5, 1.38 (1.33−1.43); C_2-N_3, 1.35 (1.31−1.40); N_3-C_4, 1.37 (1.31−1.41); and C_4-C_5, 1.35 (1.30−1.41). Ring bond angles (in degrees) were fixed as follows: N_1, 106 (102−109); C_2, 112 (107−115); N_3, 106 (105−110); C_4, 104 (103−110); and C_5, 111 (107−113). The adjustable parameters were r(Fe−N_1), $\phi = \angle$Fe−N_1−C_2, and θ (angle of the Fe−N bond with the imidazole plane). In the model structures, these parameters ranged from 1.95 to 2.23 Å, 122 to 131°, and 168 to 180° (except for one of the 61 examples which had $\theta = 163°$), respectively. For the refinements on the Fourier transform, ϕ and θ were constrained to lie within the 122−131 and 168−180° ranges.

The outer-sphere scattering due to carbon bonded to a thiolate sulfur was modeled assuming an S−C bond distance of 1.77 and allowing $\angle$Fe−S−C to vary. The multiple scattering due only to first-sphere scatterers (S_2-N_3-O and the iron itself) was calculated assuming idealized 90 and 180° X−Fe−X angles and either *trans* or *cis* disposition of the sulfur atoms (in the latter case, the nitrogen atoms were assumed to be *fac*). The nitrogen and oxygen bond lengths were assumed to be identical.

To perform the least squares optimizations of the various geometrical and disorder parameters, FEFF simulations were performed for individual structural features (imidazole rings, Fe−S−C, and multiple scattering from the first coordination sphere). The simulations were performed for a reference geometry and for geometries in which one or two parameters had been changed by small increments. These calculations were used to determine various first and second partial derivatives (including mixed second partial derivatives) for the calculated EXAFS so that it could be parameterized as a function of the Fe−X distances, the Debye temperature, and (for imidazole) the angles θ and ϕ. It was verified (by further calculations using FEFF) that the expansion in terms of partial derivatives was good for the range of parameters

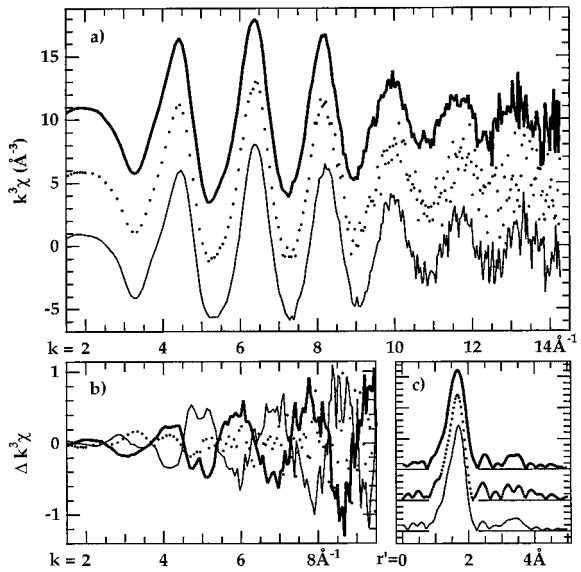

FIGURE 1: Comparison of the EXAFS of nitrile hydratase frozen at pH 7.3 (heavy line), 7.8 (dots), and 9.0 (line): (a) $k^3\chi$ + offset (10 Å^{-3} for pH 7.3; 5 Å^{-3} for pH 7.8), (b) difference spectra [$k^3\chi$ − (average of the three spectra)], and (c) Fourier transform of $k^3\chi$ between 1.0 and 14.3 Å^{-1}; succesive spectra are offset.

obtained from the least squares fitting. To account for variation in orientation among the three imidazole ligands, the outer-sphere imidazole scattering was multiplied by the Debye−Waller term $\exp(-2k^2\Delta\sigma^2_{im})$, where $\Delta\sigma^2_{im}$ is a refined parameter constrained to be non-negative. Least squares fitting showed that no significant improvement in the fit could be obtained by varying E_0 from 7125 eV. Seven parameters were allowed to vary for the reported outer-sphere fits ($n_{idp} = 16.3$); because θ, ϕ, and $\Delta\sigma^2_{im}$ were each partially constrained (see above), n_p was reduced by 1 and taken as 6 for calculation of ϵ_ν^2 (except for fits in which imidazole scattering was omitted; for these, $n_p = 4$).

RESULTS AND DISCUSSION

We report XAS analyses of fluorescence-detected K-edge iron XAS obtained at ca. 30 K of three samples of nitrile hydratase, frozen in buffers with pH values of 7.3, 7.8, and 9.0 (at 4 °C). We also report the XANES (near-edge) spectrum of a frozen pH 7.8 sample which was measured using a higher-resolution Si 220 monochromator. All samples contained 40 mM sodium butyrate as a stabilizer of the enzyme (Nagasawa et al., 1986). Butyrate is a competitive inhibitor of nitrile hydratase from *Rhodococcus* sp. R312 with a K_I of approximately 2 mM. Consequently, these samples, and all those used in previous spectroscopic studies of the enzyme (Nagasawa et al., 1986; Sugiura et al., 1987; Nelson et al., 1991; Jin et al., 1993), are of a "butyrate-inhibited" form. The pH 7.3 (low-pH) form is immediately active on dilution into assay buffer, while the pH 9.0 (high-pH) form is not (Brennan et al., 1996).

First-Sphere EXAFS Analysis

Figure 1 shows that the EXAFS changes are slight on going from the low-pH to high pH form of nitrile hydratase. Except below $k = 4$ Å^{-1} (where errors in fitting the baseline may be important), the pH 7.8 sample is intermediate between the pH 7.3 and 9.0 spectra (see Figure 1b), consistent with indications from EPR that the pH 7.8 sample contains significant amounts of both low- and high-pH forms of the enzyme.

Table 1: First-Sphere Fits to the EXAFS of Nitrile Hydratase and Model Complexes[a]

data set	fit type[b]	ϵ_ν^2	n_S (=6 − n_N)	r_S (Å)	r_N (Å)	$\Delta\sigma^2_S$ (pm^2)		$\Delta\sigma^2_N$ (pm^2)
NH, pH 7.3	raw	3.2	1.9(11)	2.214(19)	1.997(25)		0(30)[c]	
	FF1	1.7	2.4(5)	2.212(10)	1.998(16)		9(12)[c]	
	FF2	1.4	2.7(6)	2.212(9)	2.002(15)	21(19)		−4(19)
NH, pH 7.8	raw	8.4	1.5(11)	2.20(3)	2.003(26)		0(30)[c]	
	FF1	3.0	2.3(4)	2.198(11)	2.003(17)		12(11)[c]	
	FF2	2.2	2.7(5)	2.200(10)	2.008(15)	32(22)		−11(21)
NH, pH 9.0	raw	2.8	2.2(15)	2.191(23)	2.00(4)		10(30)[c]	
	FF1	1.2	2.4(4)	2.191(10)	2.001(17)		12(10)[c]	
	FF2	1.3	2.5(5)	2.191(10)	2.003(17)	17(20)		5(22)
$Fe(dedtc)_3$	raw	16.4	6.0(13)	2.307(6)	ni[d]	14(12)		ni[d]
	FF	7.7	6.1(5)	2.316(3)	ni[d]	16(8)		ni[d]
	xtal[e]		6	2.31				
FeL_1	raw	15.0	2.1(11)	2.326(20)	2.08(3)		10(30)[c]	
	FF1	2.5	2.3(6)	2.302(15)	2.106(23)		33(13)[c]	
	FF2	2.2	2.0(6)	2.305(12)	2.096(22)	14(26)		50(30)
	FF3	3.7	3	2.299(13)	2.121(27)	45(21)		40(50)
	xtal[f]		3	2.28	2.07			
FeL_2	raw	4.2	3.2(14)	2.333(13)	2.26(10)		11(16)[c]	
	FF1	3.4	3.0(4)	2.328(8)	2.25(3)		8(11)[c]	
	FF2	2.4	2.6(5)	2.342(8)	2.24(5)	−6(13)		130(100)
	FF3	2.7	3	2.341(11)	2.26(4)	2(8)		10(120)
$Fe(MeIm)_6^{2+}$	raw	8.4	6.0(26)	ni[d]	2.201(15)	ni[d]		−5(26)
	FF	5.6	5.8(8)	ni[d]	2.200(7)	ni[d]		−9(16)
	xtal[g]		6		2.20−2.21			

[a] Numbers in parentheses indicate estimated uncertainty of last reported digit. [b] "Raw" fits are to unfiltered data and "FF*x*" refinements to Fourier-filtered data; "xtal" indicates values from X-ray crystal structures. [c] $\Delta\sigma^2$ constrained to be equal for both the S and N shells. [d] ni indicates shell not included. Attempts to refine a shell of (6 − n_S) N for $Fe(dedtc)_3$ were unsuccessful; n_S tended toward 6.0, and r_N then diverged. [e] Low-temperature (77 K) crystal structure (Leipoldt & Coppens, 1973). [f] Room-temperature structure (Beissel et al., 1993). [g] EXAFS of BF_4^- salt was obtained; crystal structures are with other anions (Miller et al., 1989; Seel et al., 1980).

Scheme 1: Model N_3S_3 Ligands Used for This Study (Beissel et al., 1993)

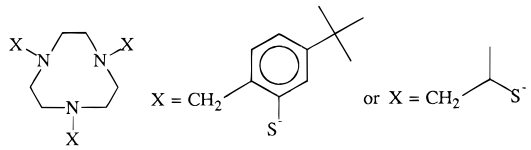

L1 **L2**

Initial fits to the EXAFS of the pH 7.8 sample required at least two atoms of the second period (N or O) and at least two atoms of the third period (S or Cl) at bonding distances from the iron (Nelson et al., 1991). On the basis of low-spin state, these were assumed to be (at least predominantly) Fe−N and Fe−S bonds. Table 1 reports two-shell fits to the unfiltered (raw) and Fourier-filtered (FF1 and FF2) EXAFS of several states of nitrile hydratase and some model complexes (Scheme 1). In these fits, $n_S + n_N$ was constrained to be 6 on the basis of low-spin state, but n_S was refined. Fits with fixed integral n_S and n_N values (FF3 fits and fits in Table 2) were also performed in order to get best estimates for Fe−X distances and disorder assuming a given coordination model. The bond lengths obtained for FeL_1 are significantly longer than the 2.07 Å average Fe−N and 2.28 Å average Fe−S distances seen in its crystal structure (Beissel et al., 1993); the difference may be due to the presence of a greater quantity of the high-spin form of the complex caused by or allowed by the powdering of the crystalline sample prior to EXAFS measurements.

Number of Bound Sulfur Atoms. In the Fourier-filtered fits to the EXAFS of nitrile hydratase at each pH, n_S was refined to be between 2 and 3; the result was closer to 2 sulfurs when the $\Delta\sigma^2$ values were constrained to be the same for Fe−N and Fe−S shells (FF1 fits of Table 1) and closer to 3 when the $\Delta\sigma^2$ values were allowed to be different (FF2 fits). Table 1 also shows EXAFS analyses carried out in the same manner for data from model complexes FeL_1 (predominantly low-spin) and FeL_2 (high-spin), both of which have N_3S_3 ligand sets (Beissel et al., 1993). Refinement of n_S gives values between 2 and 3, but for FeL_1, the value refines closer to 2 than the correct value of 3. We note that constraining the $\Delta\sigma^2$ disorder parameter to be equal for the Fe−N and Fe−S shells (FF1 fits) causes n_S to refine closer to the correct value of 3.0 for both FeL_1 and FeL_2, compared with results from fits where the $\Delta\sigma^2$ is varied (FF2 fits), and that, when the $\Delta\sigma^2$ values are allowed to refine independently, the disorder factor for nitrogen refines to a large value [compared, for example, to that for the $Fe(MeIm)_6^{2+}$ model], even though the crystal structure for FeL_1 shows that all Fe−N bond lengths are within 0.01 Å of the mean value (Beissel et al., 1993). It appears that correlation between refined n_S and the $\Delta\sigma^2$(N) parameters causes both parameters to refine to incorrect values. This would suggest that, for nitrile hydratase samples, results from FF1 fits, in which n_S refines closer to 2, are more reliable than the results from the better (lower ϵ_ν^2) FF2 fits, in which n_S refines closer to 3. However, for nitrile hydratase, it is more likely than for the models that the bond lengths actually are significantly disordered in one or the other of the shells, and so we conlcude that either two or three sulfur ligands to the iron are consistent with our EXAFS data from nitrile hydratase.

Although the difference in EXAFS scattering between nitrogen and oxygen is minor, the quality of fits, refined bond lengths, and BVS (see below) do change slightly depending on whether scatterers are modeled as nitrogen or oxygen. Table 1 fits assume all non-sulfur ligands are nitrogen, while fits shown in Table 2 assume one oxygen scatterer to account for the EPR line broadening by ^{17}O. Models A−D of Table

Table 2: Selected Fits to the First-Sphere Fourier-Filtered EXAFS of Nitrile Hydratase[a]

model	pH 7.3	pH 7.8	pH 9.0	$\Delta\sigma^{2b}$	BVS[c]
(A) 2 S, 4 N/O[d]					
r_S	2.213(10)	2.199(11)	2.191(10)	1(10)	
$r_{N/O}$	1.988(12)	1.993(12)	1.988(13)	10(16)	
ϵ_ν^2, BVS	2.6	3.3	2.0		4.23
(B) 3 S, 3 N/O[d]					
r_S	2.208(10)	2.196(11)	2.187(10)	30(12)	
$r_{N/O}$	2.000(15)	2.005(14)	2.005(16)	2(21)	
ϵ_ν^2, BVS	1.2	1.9	1.7		4.41
(C) 3 S, 4 N/O[d]					
r_S	2.198(10)	2.184(11)	2.178(10)	31(15)	
$r_{N/O}$	2.015(15)	2.019(14)	2.019(15)	32(29)	
ϵ_ν^2, BVS	1.3	1.8	1.0		5.02
(D) 2 S, 3 N/O[d]					
r_S	2.220(9)	2.209(10)	2.200(10)	−5(9)	
$r_{N/O}$	1.980(10)	1.983(11)	1.977(12)	−19(13)	
ϵ_ν^2, BVS	1.6	2.4	1.2		3.59
(E) 2 S, 3 N, 1 O					
r_S	2.213(10)	2.198(11)	2.191(10)	1(9)[e]	
r_N	$2.02(^{+2}_{-5})$	$2.02(^{+2}_{-5})$	$2.02(^{+2}_{-6})$	[e]	
r_O	$1.93(^{-3}_{+11})$	$1.94(^{-4}_{+10})$	$1.92(^{-3}_{+13})$	[e]	
ϵ_ν^2, BVS	2.2	3.0	1.5		4.18
(F) 2 S, 4 − x N/O,[d] x N_{NO}[f]					
r_S	2.217(9)	2.204(11)	2.195(9)	−1(8)	
$r_{N/O}$	1.983(10)	1.987(12)	1.982(13)	1(16)	
x	0.23(21)	0.23(22)	0.20(23)		
r_N(NO)	1.67(11)	1.66(11)	1.61(11)	0[f]	
ϵ_ν^2, BVS	2.6	3.9	2.2		4.46

[a] Distances are in angstroms; $\Delta\sigma^2$ is in squared picometers. Numbers in parentheses indicate estimated uncertainty of the last reported digit. [b] Refined $\Delta\sigma^2$ is given for fits at pH 7.3; the refined $\Delta\sigma^2$ values of other samples are within estimated uncertainty of these values. [c] Underlined values are averages of BVS values calculated from the refined distances for each sample. For all fits, the BVS values for samples at pH 7.3 and 9.0 are 0.06 ± 0.01 smaller and larger, respectively, than this average value. [d] N/O indicates a shell comprised of n − 1 nitrogen atoms and 1 oxygen atom (to account for the EPR broadening by ^{17}O). [e] $\Delta\sigma^2$ constrained to be equal for all shells to reduce parameter correlations. [f] Assumes fractional occupancy of NO ligand, with $\Delta\sigma^2$ for this Fe−N bond fixed at 0 to reduce parameter correlations.

2 are the best fits of all possible combinations with one shell of one oxygen plus n_N nitrogen atoms, all at the same distance from iron, and a second shell of n_S sulfur atoms. The possibility of $n_S < 2$ or $n_S > 3$ is precluded because $\epsilon_\nu^2 > 6$ for all models with $n_S = 1$ and $\epsilon_\nu^2 > 11$ when $n_S = 4$. Comparison of models B−D shows that roughly equally good fits to the EXAFS can be obtained assuming five, six, or seven coordination.

Model B (three sulfurs) gives a better fit than model A (two sulfurs). For the pH 7.3 and 7.8 samples, the difference in ϵ_ν^2 is greater than 1, which is considered a significant difference (Bunker et al., 1991). However, if the $\Delta\sigma^2$ values are contrained equally for the two shells, the difference in ϵ_ν^2 between models A and B is no longer significant (2.4 vs 1.8 for the pH 7.3 sample). Since our EXAFS analysis cannot establish the precise ratio of sulfur to nitrogen ligands in FeL_1 and FeL_2, we conclude that EXAFS fits are consistent with either two or three Fe−S bonds in nitrile hydratase.

BVS Analysis and Determination of the Coordination Number of Iron. We have previously used bond valence sum (BVS) analysis (Brown & Altermatt, 1985) together with EXAFS-derived bond lengths to help determine the coordination number of the high-spin iron in various states of lipoxygenase (Scarrow et al., 1994; Nelson et al., 1995). This analysis involves using bond lengths and a reference Fe−X distance (r_o; see Experimental Procedures) to estimate the "valence" of each bond; with an appropriately chosen r_o, the sum will approximate the oxidation state of the iron. In our past work and that of others (Brown & Altermatt, 1985; Thorp, 1992; Liu & Thorp, 1993), only high-spin iron complexes have been considered, and different sets of r_o have been chosen for each oxidation state to (artificially) improve the agreement between BVS and the oxidation state.

In Table 3, we tabulate results of BVS calculations on over 1000 iron coordination sites found in the Cambridge Structure Database. To avoid obscuring the real differences in size between ions of different oxidation and spin states, we used for all complexes the same set of r_o values, which are based on values originally proposed for Fe^{3+} (Brown & Altermatt, 1985). [Use of "improved" values of r_o (Liu & Thorp, 1993) for high-spin Fe^{3+} gave slightly larger ranges and esds of BVS and so was rejected.] For each class of iron compound, a bell-shaped distribution of BVS values was found. A few compounds were found to have highly anomalous BVS values which may be due to a rigid ligand environment which causes anomalous Fe−X bond lengths or to errors in either the crystal structure determination or spin state assignment.[2] In Table 3, we indicate ranges which include 98% of the coordination sites of each class and suggest that these are appropriately conservative for assign-

[2] The largest deviation is found in Fe($T^{OMe}PP$)(SH), which is low-spin by Mössbauer and NMR spectroscopy and by magnetic susceptibility of a bulk sample (English et al., 1984), but the BVS based on the crystal structure (3.10) is highly anomalous for low-spin iron(III). This may be because the porphyrin macrocycle does not allow the Fe−N bonds to shorten as predicted by BVS theory, but the large deviation from the BVS found for other $S = {}^1/_2$ complexes (and good match with that found for $S = {}^5/_2$ complexes) calls for verification of the identity of the bulk material with the single crystal.

Table 3: Ranges of BVS Values Calculated for Various Classes of Iron Complexes Based on Bond Distances from the Cambridge Structure Database and Using BVS Reference Distances (r_o) Derived from High-Spin Ferric Complexes

class	CN[a]	min−max	mean ± esd	98% range	$n_{98\%}/n$[b]
$S = {}^5/_2$ (Fe^{3+})	4, 5, 6, 7	2.49[c] to 3.37[d]	3.04 ± 0.12	2.70−3.30	608/618
$S = {}^1/_2$ (Fe^{3+})[e]	5, 6	3.10[f] to 4.69[g]	4.10 ± 0.23	3.68−4.46	85/87
$S = 2$ (Fe^{2+})	4, 5, 6, 7	1.90[h] to 2.76[i]	2.30 ± 0.14	2.03−2.69	223/228
$S = 0$ (Fe^{2+})	5, 6	3.41[j] to 4.92[k]	4.22 ± 0.34	3.67−4.84	111/114

[a] Coordination numbers considered in class. Three-coordinate complexes are excluded from the high-spin classes because the BVS values fall below the range of other compounds. Four-coordinate compounds of the type $\{Fe(NO)_2\}^9$ are not included in the $S = {}^1/_2$ class because the BVS for the four-coordinate $S = {}^1/_2$ complexes is higher (4.6 ± 0.3). [b] $n_{98\%}$ indicates the number of coordination sites which fall in the "98% range", from a total of n sites examined for the class. Structure searches were restricted to "error free" structures with $R < 10\%$. [c] $Fe(S_2P(OCH(CH_3)_2)_2)_3$ (Drew et al., 1986). [d] $[Fe(NCS)_6]^{3-}$ (Muller, 1977). [e] Includes $\{FeNO\}^7$ complexes, which are Fe^{3+} if nitric oxide is considered to bind as NO^-. These account for all but one (note *f*) of the 12 five-coordinate members of this class. [f] $Fe(T^{OMe}PP)(SH)$ (English et al., 1984). [g] $Fe(MTG)_2^-$ (Ryabova et al., 1979). [h] Nominally five-coordinate iron in tris[[*N*,*N*′-dimethyl-*N*,*N*′-bis(2-mercaptoethyl)-1,3-propanediamine-*N*,*N*′,*S*,*S*]nickel]iron(2+) (Colpas et al., 1992). [i] Battioni et al. (1986). [j] Fe(TPP)(piperidine)$_2$ (Radonovich et al., 1972). [k] The cage complex bis(phenylborato)tris(1-phenylethane-1,2-diimine)iron (Zavodnik et al., 1993).

ment of the oxidation or spin state or coordination number from the BVS calculated from a crystal structure or an EXAFS analysis.

Comparing the BVS values from Table 2 with the range of 3.68−4.46 found in 98% of low-spin ferric complexes, it is apparent that the BVS is appropriate for all six-coordinate fits in Table 2 but is too big for the seven-coordinate fit (model C) and too small for the five-coordinate fit (model D). Thus, the possibilities of a novel five- or seven-coordinate low-spin iron center in nitrile hydratase can be eliminated on the basis of the BVS analysis of the EXAFS-derived bond lengths.

From EPR line broadening (Sugiura et al., 1987) and ENDOR spectroscopy (Jin et al., 1993), it is known that a solvent exchangeable oxygen atom binds iron in nitrile hydratase and that three nitrogens coordinate the iron. These four ligands account for the four-N/O shell of model A in Table 2, and because the EXAFS analysis requires at least two Fe−S bonds, and the BVS analysis implies overall six coordination, the identity of the ligands is established as N_3S_2O.

As mentioned above, all spectroscopic investigations of nitrile hydratase (including the present study) have used butyrate to stabilize the enzyme. Because nitrile hydratase lacks amidase activity, it would not be expected to catalyze ^{17}O exchange into butyric acid from water. Since the above analysis does not allow for a second, non-solvent exchangable oxygen ligand to the iron, we conclude that butyrate does not coordinate the iron site.

Possibility of OH or NO Coordination in Nitrile Hydratase. Although N and O scatterings are very similar, one can distinguish them if the Fe−O bond is considerably shorter than the Fe−N bonds, so that separate shells are resolved by the EXAFS. This occurs, for instance, in the ferric (active) form of lipoxygenase where one Fe−O bond is much shorter than the other Fe−O/N bonds and thus could be assigned to a hydroxide ligand (Scarrow et al., 1994). To investigate this possibility for nitrile hydratase, we attempted fits with three shells in the first sphere: one short Fe−O bond, three slightly longer Fe−N bonds, and two Fe−S bonds. To reduce the number of refined parameters, $\Delta\sigma^2$ was kept the same for all shells. These fits are shown in Table 2 (model E). The fits (judged by ϵ_ν^2) are generally slightly better than the model A fits, but not enough so to conclude definitively from the EXAFS that the Fe−O bond length is distinct from (and shorter than) the Fe−N bond lengths.

Because nitrile hydratase is a low-spin complex, the relative uniformity of the Fe−N and Fe−O bond lengths does not rule out hydroxide coordination. In high-spin iron(III) complexes, Fe−$^-$OR bonds are ca. 0.2 Å shorter than Fe−N bonds, but the difference is much smaller in low-spin complexes. This is illustrated dramatically in a series of 1:2 complexes of iron(III) and substituted tsa (Ryabova et al., 1978, 1981, 1982a,b). These complexes exhibit spin-crossover behavior. For complexes and temperatures where the high-spin state predominates, the difference between the average Fe−$^-$OR bond length and the average Fe−N bond length is 0.10 Å. For low-spin forms, the difference is only 0.02−0.03 Å. Thus, for a low-spin FeN_3OS_2 coordination environment, the Fe−O bond need not be significantly shorter than the Fe−N bonds, even for an alkoxide/hydroxide ligand. A corollary of this result is that, if the difference between the low-pH and high-pH forms of nitrile hydratase were deprotonation of $Fe-OH_2$, the change in ligand field would not be detectable by the EXAFS because the average bond lengths of the Fe−N(O) shell would change only slightly.

The EXAFS analysis is not compatible with the possibility that NO is stoichiometrically bound to iron in the active form of nitrile hydratase from *Rhodococcus* sp. R312. This was suggested on the basis of the FTIR difference spectrum between the dark-adapted and active forms of nitrile hydratase from *Rhodococcus* sp. N-771, in which at least one metal-bound NO stretching frequency is identified for each of the enzyme forms (before and after light activation) (Noguchi et al., 1995). As shown in Table 2 (model E), the uncertainty ranges for the Fe−O distances in the three-shell fits are asymmetric about the optimal value; fits within 1 of the minimal ϵ_ν^2 may be obtained for r_{FeO} between 1.90 and about 2.05 Å. Thus, the shortest bond distance in nitrile hydratase is somewhere between 1.90 and 1.99 Å. This is much longer than the Fe−N bond distance (1.6−1.8 Å) expected if nitric oxide were coordinated to the iron in nitrile hydratase.[3] Therefore, there is no evidence for stoichiometric coordination of NO to the iron in these samples. The EXAFS does allow for the possibility of ca. 20% of the iron

[3] The suggested Fe−NO complex in active nitrile hydratase would be classified as a $\{FeNO\}^7$ complex because it exhibits an $S = {}^1/_2$ EPR spectrum (Enemark & Feltham, 1974). Included in the $S = {}^1/_2$ category of Table 4 are three such six-coordinate complexes with Fe−NO bond lengths of 1.74−1.75 Å (Sellmann et al., 1988; Scheidt et al., 1977; Scheidt & Piciulo, 1976). Also included are 11 five-coordinate $\{FeNO\}^7$ complexes with Fe−NO bond lengths of 1.64−1.79 Å.

Table 4: Average M−S Distances ($r_{S_{av}}$) in Pseudo-Octahedral and Square Planar Complexes of First-Row Transition Metals Ligated by Two Sulfur Atoms and Four or Two Oxygen and/or Nitrogen Atoms[a]

	$r_{S_{av}}$ (Å) for *cis*-S−M−S		$r_{S_{av}}$ (Å) for *trans*-S−M−S	
ion[b]	mean ± esd	(range; *n*[c])	mean ± esd	(range; *n*)
Cr^{3+} (6)	2.39 ± 0.02	(2.37−2.42; 3)	2.40 ± 0.01	(2.39−2.42; 4)
Fe^{3+} (ls, 6)	2.23 ± 0.02	(2.20−2.26; 6[d])	2.33 ± 0.03	(2.29−2.38; 9)
Fe^{2+} (ls, 6)	2.26 ± 0.03	(2.24−2.28; 2)	2.33 ± 0.02	(2.31−2.34; 3)
Co^{3+} (ls, 6)	2.24 ± 0.02	(2.20−2.28; 54)	2.29 ± 0.03	(2.23−2.35; 22)
Co^{2+} (hs, 6)	2.53 ± 0.05	(2.46−2.64; 11)	2.57 ± 0.06	(2.49−2.67; 9)
Ni^{2+} (ls, 4)	2.16 ± 0.02	(2.12−2.25; 104)	2.19 ± 0.02	(2.15−2.24; 31)
Ni^{2+} (hs, 6)	2.43 ± 0.07	(2.31−2.69; 60)	2.46 ± 0.05	(2.38−2.58; 18)
Cu^{2+} (4)	2.26 ± 0.03	(2.23−2.36; 16)	2.28 ± 0.03	(2.25−2.36; 17)
Cu^{2+} (6, equatorial S[e])	2.33 ± 0.03	(2.30−2.36; 5)	2.39 ± 0.03	(2.37−2.45; 6)
Cu^{2+} (6, axial S[f])	2.52 ± 0.06	(2.43−2.62; 9)	2.89 ± 0.14	(2.71−3.17; 20)

[a] Search of error free structures in CSD containing $MS_2(N \text{ or } O)_{2 \text{ or } 4}$ coordination units and two or three X−M−X angles of 150−180°. Mean, esd, and ranges are calculated from $r_{S_{av}}$ rather than from the individual r_{M-S} bond lengths. [b] High- or low-spin state and coordination number shown in parentheses. [c] Number of coordination environments in CSD; crystallographically independent units and structues at multiple temperatures are counted separately. [d] Includes $[Fe(ADIT)_2]^+$ (Shoner et al., 1995) which was not found in the CSD search. [e] Axially elongated structures with both Cu−S bonds in the equatorial plane; these complexes invariably have axial Cu−O bonds. [f] Axially elongated structures with one or two S in an axial position.

being in an NO-bound form with $r = 1.6-1.7$ Å for the Fe−NO bond. The refinements based on an assumption of fractional NO binding, shown in Table 2 (model F), should **not** be interpreted as evidence for partial binding of NO to iron. The refined uncertainty range for the fraction of the NO-bound form includes zero, and the addition of refined parameters increases (at pH 7.8 and 9.0) the fit index in model F compared to that in model A. Thus, the EXAFS indicates either no NO binding or that NO binds to only a minor fraction of the iron sites in nitrile hydratase as we have prepared the enzyme.

Fe−S Bond Lengths. The refined Fe−S bond lengths in nitrile hydratase (2.19−2.21 Å) are as short as any six-coordinate iron(III)−thiolate bond lengths found in small molecule crystal structures and are shorter than any iron(III)−thioether bonds, supporting the assignment of cysteine rather than methionine ligation to explain the Fe−S bonds.[4] The bond lengths are virtually identical to those found recently in $[Fe(ADIT)_2]^+$ which closely mimics the EPR and visible spectra of nitrile hydratase (Shoner et al., 1995). The mutually *cis* Fe−S bonds have $r_{S_{av}} \equiv (r_{Fe-S_1} + r_{Fe-S_2})/2 = 2.20$ Å. Four other complexes were found in the Cambridge Structure Database with two *cis* sulfur ligands and four N/O atom ligands to low-spin iron(III) (complexes exhibiting spin-crossover behavior at 300 K were excluded). In these complexes, $r_{S_{av}}$ ranges from 2.21 Å in bis[*N*-(2-aminoethyl)-thiosalicylideneiminato]iron(III) chloride (Fallon & Gatehouse, 1975) to 2.25 Å in $Fe(MTG)_2^-$ (Ryabova et al., 1979). These three structures have S_2N_4 donor atom sets; each sulfur is *trans* to nitrogen. Low-spin $[Fe(5\text{-Cl-tsa})_2]^-$ (at both 135 and 298 K) and $[Fe(5\text{-Br-tsa})_2]^-$ have $r_{S_{av}} = 2.23$ Å; in these cases, the sulfur atoms are *trans* to the oxygen atoms (Ryabova et al., 1978, 1981).

[4] The shortest Fe^{3+}−thioether bond in the CSD is 2.25 Å in bis[1,4-bis(2′-mercaptophenyl)-1,4-dithiabutanato](μ-disulfido)diiron(III) (Sellmann et al., 1991). In this complex, iron−thioether bonds are shorter by ca. 0.04 Å than the iron−thiolate bonds; this is probably due to steric compression caused by the thioether sulfur's participation in two five-membered chelate rings with the same metal ion. Such five-membered chelate rings cannot be formed by the thioether group of methionine. The seven iron(III) complexes with *trans*-S_2N_4 ligation used in Table 4 (where the Fe−S bonds are not part of chelate rings) confirm the expected trend that iron-thiolate bonds are shorter than iron−thioether bonds; four complexes with Fe−thiolate bonds have $r_{S_{av}} = 2.29-2.34$ Å, while three complexes with Fe−thioether bonds have $r_{S_{av}} = 2.34-2.38$ Å.

We also searched the Cambridge Structure Database for low-spin ferric complexes with a *trans*-$(S)_2(N \text{ or } O)_4$ ligand atom set, and found seven complexes (all S_2N_4), with $r_{S_{av}}$ from 2.29 Å for $[Fe(TIM)(SCH_2Ph)_2]^+$ (Aruffo et al., 1984) to 2.38 Å for $[Fe(TPP)(\text{tetrahydrothiophene})_2]^+$ (Mashiko et al., 1981). These distances are all larger than those in the five *cis*-$(S)_2(N \text{ or } O)_4$ models mentioned above. The lack of overlap between $r_{S_{av}}$ ranges for *cis*-S and *trans*-S low-spin iron(III) complexes is possibly coincidental due to the small number of crystal structures of these types which have been obtained to date. However, it appears to be generally true for first-row transition metal complexes with two sulfur atom ligands (and otherwise N/O ligands) that the shortest $r_{S_{av}}$ values are observed for complexes with mutually *cis* M−S bonds (Table 4). Further evidence for a tendency for pairs of M−S bonds to be shorter when they are *cis* is provided by cases where different stereoisomers have been crystallized. Defining $\Delta r_{S_{av}} \equiv r_{S_{av}}$ (*trans*-S isomer) − $r_{S_{av}}$ (*cis*-S isomer) (and averaging the values of $r_{S_{av}}$ where there is more than one *trans*-S or *cis*-S structure), $\Delta r_{S_{av}} = 0.04$ Å for $[Co(\text{L-Met})_2]^+$ (Hambley, 1988), $\Delta r_{S_{av}} = 0.02$ Å for bis(1-thia-4,7-diazacyclononane)cobalt(3+) (Hambley et al., 1989; Hambley & Gahan, 1986), $\Delta r_{S_{av}} = 0.05$ Å for $[Co(en)_2(SO_3)_2]^-$ (Raston et al., 1979; Fallon et al., 1980), $\Delta r_{S_{av}} = 0.02$ Å for bis(thiosemicarbazide)nickel(2+) (Gronbaek & Rasmussen, 1962; Hazell, 1968, 1972), and $\Delta r_{S_{av}} = 0.04$ Å for bis(thioacetohydroxamato)nickel (Sato et al., 1968, 1969).

This evidence from the crystallographic data base suggests an electronic reason, perhaps involving π-bonding between the first-row transition metal and the sulfur atoms, which causes *cis*-S−M−S bonds to be somewhat shorter than *trans*-S−M−S bonds. This effect has been noted before for cobalt(III) complexes and ascribed to a weak *trans* effect of sulfur ligands (Hambley, 1988; Hambley et al., 1989). The available structures of $FeS_2(N \text{ or } O)_4$ complexes (discussed above) indicate that this trend holds, and is perhaps accentuated, for low-spin ferric complexes.[5] Thus, the short EXAFS-derived Fe−S bond lengths for nitrile hydratase are strong support for the presence of mutually *cis* cysteine thiolate ligands to the iron. This corroborates the earlier interpretation of ENDOR spectra in favor of *cis*-thiolate coordination in nitrile hydratase (Jin et al., 1993).

Changes in the Iron Site with pH. There are slight but significant changes in both the EXAFS and the refined parameters as a function of the pH of the nitrile hydratase solution. The clearest change is in the Fe−S distance, which shortens by about 0.02 Å on going from pH 7.3 to 9.0 (Tables 1 and 2). We have employed a conservative method of estimating parameter uncertainties (Bunker et al., 1991). Comparing uncertainty ranges from the same types of fits, we conclude that the shortening of the average Fe−S bond distance is between 0.002 and 0.04 Å, with the most likely values between 0.01 and 0.03 Å. This could be due to both Fe−S bonds contracting equally or to one Fe−S bond staying the same and the other shortening by a larger amount. This change in bond length is also predicted from changes in the Raman spectrum (Brennan et al., 1996). A plausable explanation for the pH dependent change is that at least one of the coordinated cysteine thiolate sulfur atoms accepts a hydrogen bond from a donor group which deprotonates with p$K_a \approx 8$. Upon losing the hydrogen bond, the sulfur−iron bond would be expected to strengthen. As mentioned above, we cannot from the EXAFS eliminate the possibility of a coordinated water deprotonating with p$K_a \approx 8$, but we have no support for this possibility either.

Outer-Sphere and Multiple Scattering Contributions to the EXAFS

The unfiltered EXAFS is fit well but not perfectly by first sphere models (Figure 2). The Fourier transform (Figure 1c) does not indicate a strong scatterer beyond the first coordination sphere (such as another metal ion held at a rigid distance as part of a cluster). The weak intensity in the Fourier transform above $r' = 2.5$ Å is similar to that which is frequently attributed to multiple scattering by imidazole ligands in metalloproteins.

Scattering Pathways Contributing to the High-Frequency EXAFS. We tested the hypothesis that the high-frequency EXAFS of nitrile hydratase is caused primarily by the three imidazole ligands implicated by ENDOR (Jin et al., 1993). The multiple scattering simulation program FEFF 6 (Mustre de Leon et al., 1991; Rehr et al., 1991) gave good simulations of both the raw data (Figure 2) and the Fourier transform (Figure 3) when we assumed three imidazole ligands, two methane thiolate ligands (to simulate cysteine ligation), and a water.

Adding simulated EXAFS from various types of multiple scattering pathways showed that paths involving only the iron and first-sphere atoms were comparable in significance to paths involving the outer atoms on the three imidazole rings (compare Figures 3a1 and 3a3). These "first-sphere multiple scattering" (FSMS) paths include double scattering Fe−X−Y−Fe electron paths and triple scattering Fe−X−Fe−Y−Fe paths. The EXAFS from these paths was significantly different depending on whether the sulfur atoms were assumed to be *cis* or *trans*.

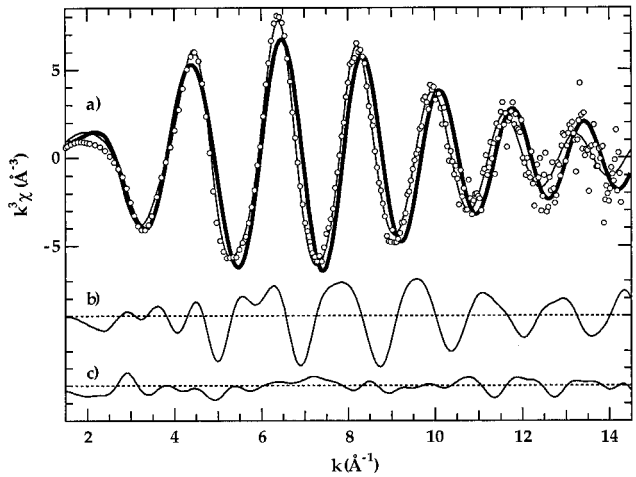

FIGURE 2: (a) Comparison of $k^3\chi$ EXAFS data for pH 9.0 nitrile hydratase (○) with the first sphere fit E of Table 2 (thick line) and a multisphere simulation using FEFF (thin line). (b and c) Difference spectra from fit E and the multisphere simulation, respectively, after noise reduction by Fourier filtering (backtransform limits $r' = 0-5$ Å). The multisphere simulation uses Fe(im)$_3$-*cis*-(SCH$_3$)$_2$(OH) as a model with refined parameters (and uncertainty ranges for last digit): $r_{FeN} = r_{FeO} = 1.996(8)$ Å, $r_{FeS} = 2.197(6)$ Å, ∠Fe−S−C$_s$ = 106(4)°, $\phi = 123°$, $\theta = 170°$, Debye temperature = 4.9(3) × 10^2, and $\Delta\sigma^2_{im} = 0.005(^{+10}_{-5})$ Å^2.

We tested three approaches to the FSMS. We calculated FSMS assuming either *cis* or *trans* orientations of the thiolate ligands (the *cis*-S and *trans*-S approaches) or neglected the predicted contributions from FSMS (the "no FSMS" approach). The collective importance of the FSMS pathways to the simulated EXAFS is enhanced, in our *cis*-S and *trans*-S simulations, by constructive interference from multiple pathways of the same lengths. This is caused by the assumptions of 90 and 180° bond angles, which are likely to be close to the true values for low-spin iron centers due to ligand field stabilization (Huheey, 1983). As the geometrical symmetry is decreased, the FSMS EXAFS is expected to decrease. Thus, the no FSMS approach may be alternatively termed a low-symmetry model.

For the pH 7.3 sample, the best fit was obtained with the *cis*-S approach (Figure 3a; $\epsilon_\nu^2 = 4.6$); the fit was "significantly" worse [ϵ_ν^2 increased by more than 1 (Bunker et al., 1991)] with the *trans*-S approach (Figure 3b; $\epsilon_\nu^2 = 6.3$) or the no FSMS approach (Figure 3c; $\epsilon_\nu^2 = 7.1$). The *cis*-S approach also gave the best fits to the pH 9.0 data ($\epsilon_\nu^2 =$ 4.0 vs 5.6 by the *trans*-S approach and 6.7 by the no FSMS approach). All the fits have residuals well above noise level ($\epsilon_\nu^2 \gg 1$); for this reason, the differences in fit appear relatively minor (Figure 3d). One identifiable reason for the relatively poor fit by the *trans*-S approach is a strong predicted contribution from the linear Fe−S$_1$−Fe−S$_2$−Fe pathway which gives rise to the predicted intensity at $r' =$ 3.9 Å (Figure 3b1); the Fourier transform magnitude of the nitrile hydratase data in this region is quite small, suggesting the absence of such a pathway. These results suggest the need for studies of FSMS effects in the EXAFS of crystallographically characterized model complexes; in the absence of such studies, the multisphere simulations of the EXAFS offer weak support for the *cis* arrangement of thiolate ligands to iron in nitrile hydratase.

[5] This effect will be accentuated if Jahn−Teller distortion (Huheey, 1983) is present, as it is in six-coordinate copper(II) complexes, because the sulfur ligands give weaker ligand fields than nitrogenous ligands and are thus favored in the longer, axial positions in the distorted complex. When this happens in Cu(II) complexes (last line of Table 4), there is a large difference in $r_{S_{av}}$ between *cis*-S complexes (where one Cu−S bond is equatorial and the other axial) and *trans*-S complexes (with two axial Cu−S bonds). Jahn−Teller distortions, although usually of small magnitude for low-spin d^5 complexes (Huheey, 1983), may accentuate the differences between the range of $r_{S_{av}}$ values observed for low-spin Fe^{3+}−*trans*-S$_2$N$_4$ complexes and the range of $r_{S_{av}}$ for the *cis*-S complexes.

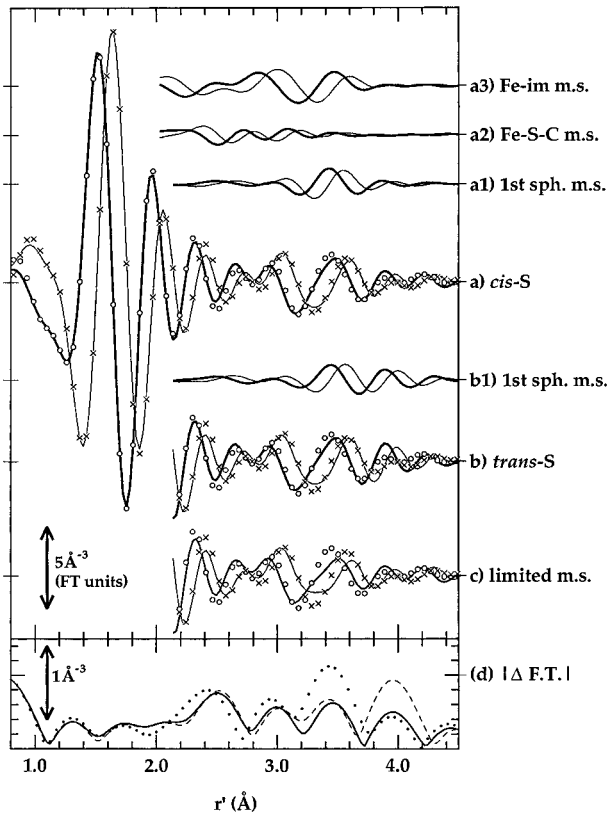

FIGURE 3: Multisphere simulations using FEFF of the EXAFS of pH 7.3 nitrile hydratase. Real (data, ○; and simulation, heavy line) and imaginary (data, ×; and simulation, light line) parts of the Fourier transform of $k^3\chi$ ($k = 2-10$ Å^{-1}) are shown. (a) Simulation using "*cis*-S" approach (see text); refined parameters (with uncertainty ranges for the last digit) are $r_{FeN} = r_{FeO} = 1.993(8)$ Å, $r_{FeS} = 2.220(6)$ Å, $\angle Fe-S-C_s = 106(2)°$, $\phi = 122°$, $\theta = 170°$, Debye temperature $= 5.2(4) \times 10^2$, and $\Delta\sigma^2_{im} = 0.006(^{+12}_{-6})$ Å^2. (b) Simulation using "*trans*-S" approach; refined parameters are the same as above except $\theta = 169°$. (c) Simulation using "no FSMS" approach; $\theta = 168°$, $\Delta\sigma^2(im) = 0.000(+6)$ Å^2 (refined value $= +0.0001$ Å^2; constrained non-negative), and the other refined parameters are the same as above. (a1−a3 and b1) High-frequency contributions from various types of multiple scattering pathways to simulations a and b. (d) Magnitude of the Fourier transform difference spectra (simulation − data) from simulations shown in a (—), b (- - -) and c (•••).

Like the first-sphere refinements, the multisphere fits predict a 0.02 Å reduction in the Fe−S distance in nitrile hydratase due to the change in the pH from 7.3 to 9.0. The refined parameters relating to the geometry of the imidazole groups (see captions to Figures 2 and 3) are virtually the same for the pH 7.3 and 9.0 data sets and were almost independent of whether the *cis*-S, *trans*-S, or no FSMS approach was employed. For the fit of Figure 3a, the calculated distances from iron to the atoms of the imidazole ring are as follows: $Fe-C_2 = 2.92$ Å, $Fe-C_5 = 3.08$ Å, $Fe-N_3 = 4.09$ Å, and $Fe-C_4 = 4.18$ Å; distances calculated for the other fits are within 0.01 Å of these values. Because of the high uncertainty in θ and ϕ, these distances are poorly determined.

In performance of the refinements and determination of uncertainty ranges, ϕ and θ were constrained to lie within ranges of 122−131 and 168−180°, on the basis of crystallographic results on small molecules (see Experimental Procedures). These parameters are highly correlated with each other and with $\Delta\sigma^2_{im}$, and their uncertainty ranges in most cases include the entire range of constraint. The values of ϕ in the fits to the pH 7.3 data (Figure 3) are at the minimum of the constrained range; when the constraint is removed, ϕ refines to 121°, $\theta = 166-167°$, and ϵ_ν^2 decreases to 3.2 for *cis*-S approach and to 5.7 for both the *trans*-S and no FSMS approaches.

We analyzed the pH 7.3 data in an attempt to confirm the number of imidazole groups bound to iron. The profiles of ϵ_ν^2 vs the number of imidazole groups included in the model (0−3) are as follows: *cis*-S, 8.9, 5.6, 4.3, and 4.6; *trans*-S, 11.2, 8.1, 6.3, and 6.3; and no FSMS, 15.2, 10.7, 7.4, and 7.1. Thus, regardless of the approach to the FSMS, fits assuming two or three imidazole groups are not significantly different, so we cannot make a precise determination of the number of imidazole groups bound from our present multiple scattering analysis. From the significantly larger ϵ_ν^2 obtained when no imidazole outer-sphere scattering is included, we conclude that at least one and probably two or three imidazole groups contribute to the high-frequency (outer-sphere) EXAFS of nitrile hydratase.

Fe K-Edge Shape

The edge region (XANES) of the iron K-edge XAS spectrum of nitrile hydratase in the presence of 40 mM butyrate is shown in Figure 4. The edge region was deconvoluted as three pre-edge absorption features (lower right, Figure 4) in the course of fitting the edge and baseline to extract the EXAFS spectrum (see Experimental Procedures). As shown by the pH 7.8 spectrum in Figure 4, these features are more pronounced in data obtained with a higher-resolution Si 220 monochromator. No pH dependent change in the XANES spectra is noted upon comparing the spectra obtained with the Si 111 monochromator (or deconvoluted peak parameters) for pH 7.3, 7.8 (not shown in Figure 4), and 9.0 samples.

The lowest-energy feature, at 7112 eV, is generally observed in spectra of iron coordination compounds and is assigned to a 1s → 3d transition. The intensity of this peak is an indicator of coordination number for high-spin ferric and ferrous complexes; symmetrical six-coordinate complexes give the smallest peak areas (Roe et al., 1984; Randall et al., 1995). A prominent shoulder at 7117 eV, as found in the XANES of nitrile hydratase, is a general feature of sulfur-containing ferric complexes (Roe et al., 1984).

For the nitrile hydratase data obtained with the Si 111 monochromator, the overlap between the 7112 and 7117 eV peaks was severe and we were unable to get a visually satisfying fit to the edge using the arctangent function used in the previous studies (Roe et al., 1984). We were more successful with the higher-resolution data; the area for the 1s → 3d pre-edge peak depends slightly on which points between $E = 7115$ and 7125 eV are used to determine the arctangent edge, but are in the range 0.10 ± 0.01 eV (see Figure 4). By the same procedure, we determined peak areas of 0.054 eV for FeL_1 and 0.084 eV for FeL_2 (cf. Scheme 1).

As discussed above, the bond lengths from the EXAFS and the low-spin state of the iron leave little doubt that the iron is in fact six-coordinate in nitrile hydratase. The relatively small 1s → 3d peak areas for six-coordinate high-spin ferric complexes (0.06−0.09 eV, excluding clusters with μ-oxo bridging ligands) are ascribed to the centrosymmetry of the pseudo-octahedral ligand field; this prevents the mixing of 4p and 3d orbitals required to make the transition dipole-

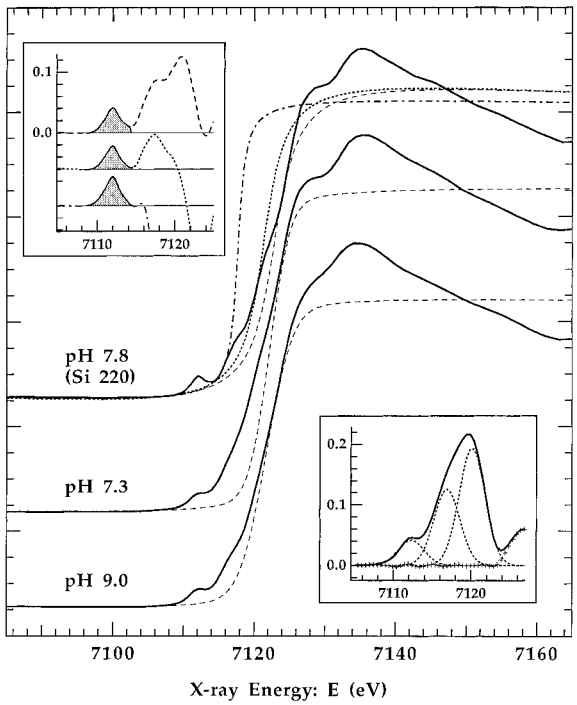

FIGURE 4: Fluorescence-detected Fe K-edge XANES (ξ_{obs}) of nitrile hydratase with 40 mM butyrate shown with the simulated edge shapes (dashed lines, which include contributions from cubic spline baselines). XAS for the pH 7.8 sample was obtained with a higher-resolution (Si 220) monochromator, and three possible arctangent-type edges (Roe et al., 1984) were determined by fitting to various regions of the pre-edge data. The upper left inset shows three determinations of $\xi_{pre} = \xi_{obs} -$ edge for the pH 7.8 data (line types correspond to the edge simulations of the main graph). The determined areas of the 1s → 3d pre-edge peak (shaded regions), in units of electron volts by edge height, are 0.101 (− −), 0.086 (- - -), and 0.112 (− - −). XAS for the pH 7.3 and 9.0 samples was obtained with a Si 111 monochromator and was deconvoluted as three Gaussian pre-edge peaks (p_1, p_2, and p_3) and an alternate edge shape (see Experimental Procedures). The lower right inset shows, for pH 7.3 data, ξ_{pre} (−), its simulation as the sum of p_1, p_2, and p_3 (- - -), and the residual, $\xi_{pre} - \sum p_i$ (+ + +). The vertical scale for insets is relative to the edge height.

allowed. Loss of centrosymmetry from short (strong) bonds *trans* to longer (weaker) bonds was noted in complexes with peak areas at the high end of the 0.06−0.09 eV range for six-coordinate monoferric complexes; the same effect explains the larger pre-edge peaks (ca. 0.15 eV) found for six-coordinate diferric complexes because these complexes have very short (1.7−1.8 Å) iron−μ-oxo bonds (Roe et al., 1984). The 1s → 3d peak area for nitrile hydratase is at, or slightly higher than, the high end of the range found for six-coordinate high-spin monoferric complexes, and it is almost twice the peak area for the predominantly low-spin FeL_1. This indicates some acentricity in the six-coordinate ligand field of the iron in nitrile hydratase; the presence of short, mutually-*cis* Fe−S bonds (see above) is a plausible explanation for this departure from octahedral centrosymmetry.

CONCLUSIONS

Our analysis of the iron K-edge XAS of nitrile hydratase and previous EPR (Sugiura et al., 1987) and ENDOR (Jin et al., 1993) studies allow the following conclusions about the coordination of iron in the "butyrate-inhibited" form of nitrile hydratase.

(1) The ligand set is N_3S_2O. EPR and ENDOR spectroscopies require at least one O-donor ligand, ENDOR spectroscopy requires at least three N-donor ligands, and the EXAFS requires at least two Fe−S bonds. The possibility of a seventh ligand is rejected because of the low-spin state, and because the bond distances obtained from the EXAFS are consistent only with six coordination, as demonstrated by the BVS analysis.

(2) The two sulfur ligands are thiolates on the basis of their short Fe−S bonds and the analysis of the Raman spectrum (Brennan et al., 1996). They are almost certainly mutually *cis* on the basis of analysis of the ENDOR spectroscopy (Jin et al., 1993) and comparisons of the M−S bond lengths to those of small inorganic complexes (cf. Table 4). The ligation of iron by *cis* thiolates also helps explain the relatively large area of the 1s → 3d pre-edge peak and the high-frequency components of the EXAFS.

(3) At least one and more likely two or three of the nitrogen ligands identified by ENDOR are from histidine side chains on the basis of the multiple scattering EXAFS analysis. Our EXAFS analysis rules out the possibility of NO coordination to iron, except perhaps as a minor and EPR-silent contaminating form of the enzyme.

(4) EPR and ENDOR establish that the oxygen ligand to the iron is solvent exchangeable, and almost certainly an aqua or hydroxo ligand. Because this is a low-spin ferric complex, bond lengths are not useful for determining whether the oxygen ligand is water or hydroxide. Because there is only a single oxygen ligand, the stabilizer butyrate, which is known to inhibit the enzyme, does not coordinate to the iron.

(5) The change in spectral properties of nitrile hydratase as pH is increased above 8 is associated with a shortening of one or both Fe−S bonds. This is consistent with the analysis of resonance Raman data (Brennan et al., 1996). The most likely explanation for this is loss of a hydrogen bond to a thiolate sulfur.

ACKNOWLEDGMENT

We thank Karl Wieghardt for the gift of compounds FeL_1 and FeL_2 and Fred Hollander (Department of Chemistry, University of California, Berkeley) for assistance with using QUEST and the Cambridge Structure Database.

REFERENCES

Allen, F. H., Davies, J. E., Galloy, J. J., Johnson, O., Kennard, O., Macrae, C. F., Mitchell, E. M., Mitchell, G. F., Smith, J. M., & Watson, D. G. (1991) *J. Chem. Inf. Comput. Sci. 31*, 187−204.

Aruffo, A. A., Santarsiero, B. D., Schomaker, V., & Lingafelter, E. C. (1984) *Acta Crystallogr., Sect. C 40*, 1693−1695.

Battioni, J.-P., Artaud, I., Dupre, D., Leduc, P., Akhrem, I., Mansuy, D., Fischer, J., Weiss, R., & Morgenstern-Badarau, I. (1986) *J. Am. Chem. Soc. 108*, 5598−5607.

Beissel, T., Buerger, K. S., Voigt, G., Wieghardt, K., Butzlaff, C., & Trautwein, A. X. (1993) *Inorg. Chem. 32*, 124−126.

Brennan, B. A., Cummings, J. G., Chase, D. B., Turner, I. M., Jr., & Nelson, M. J. (1996) *Biochemistry 35*, 10068−10077.

Briand, D., Dubreucq, E., Perrier, V., Grimaud, J., & Galzy, P. (1994) *Microbios 78*, 205−214.

Brown, I. D., & Altermatt, D. (1985) *Acta Crystallogr., Sect. B 41*, 244−247.

Bunker, G., Hasnain, S., & Sayers, D. (1991) in *X-ray Absorption Fine Structure* (Hasnain, S. S., Ed.) pp 751−770, Ellis Horwood, New York.

Colpas, G. J., Day, R. O., & Maroney, M. J. (1992) *Inorg. Chem. 31*, 5053−5055.

Drew, M. G. B., Hopkins, W. A., Mitchell, P. C. H., & Colclough, T. (1986) *J. Chem. Soc., Dalton Trans.*, 351−353.

Duran, R., Nishiyama, M., Horinouchi, S., & Beppu, T. (1993) *Biosci., Biotechnol., Biochem. 57*, 1323−1328.
Enemark, J. H., & Feltham, R. H. (1974) *Coord. Chem. Rev. 13*, 339−406.
English, D. R., Hendrickson, D. N., Suslick, K. S., Eigenbrot, C. W., Jr., & Scheidt, W. R. (1984) *J. Am. Chem. Soc. 106*, 7258−7259.
Fallon, G. D., & Gatehouse, B. M. (1975) *J. Chem. Soc., Dalton Trans.*, 1344−1347.
Fallon, G. D., Raston, C. L., White, A. H., & Yandell, J. K. (1980) *Aust. J. Chem. 33*, 665−670.
Gronbaek, R., & Rasmussen, S. E. (1962) *Acta Chem. Scand. 16*, 2325−2336.
Hambley, T. W. (1988) *Acta Crystallogr., Sect. B 44*, 601−609.
Hambley, T. W., & Gahan, L. R. (1986) *Acta Crystallogr., Sect. C 42*, 1322−1324.
Hambley, T. W., Gahan, L. R., & Searle, G. H. (1989) *Acta Crystallogr., Sect. C 45*, 864−870.
Hazell, R. G. (1968) *Acta Chem. Scand. 22*, 2171−2182.
Hazell, R. G. (1972) *Acta Chem. Scand. 26*, 1365−1374.
Huheey, J. E. (1983) *Inorganic Chemistry*, 3rd ed., Harper & Row, Philadelphia.
Ikehata, O., Nishiyama, M., Horinouchi, S., & Beppu, T. (1989) *Eur. J. Biochem. 181*, 563−570.
Jin, H., Turner, I. M., Jr., Nelson, M. J., Gurbiel, R. J., Doan, P. E., & Hoffman, B. M. (1993) *J. Am. Chem. Soc. 115*, 5290−5291.
Kobayashi, M., Nagasawa, T., & Yamada, Y. (1992) *Trends Biotechnol. 10*, 402−408.
Leipoldt, J. G., & Coppens, P. (1973) *Inorg. Chem. 12*, 2269−2274.
Liu, W., & Thorp, H. H. (1993) *Inorg. Chem. 32*, 4102−4105.
Mashiko, T., Reed, C. A., Haller, K. J., Kastner, M. E., & Scheidt, W. R. (1981) *J. Am. Chem. Soc. 103*, 5758−5767.
Mayaux, J.-F., Cerbelaud, E., Soubrier, F., Faucher, D., & Pétré, D. (1990) *J. Bacteriol. 172*, 6764−6773.
Miller, L. L., Jacobson, R. A., Chen, Y. S., & Kurtz, D. M., Jr. (1989) *Acta Crystallogr., Sect. C 45*, 527−529.
Muller, U. (1977) *Acta Crystallogr., Sect. B 33*, 2197−2201.
Mustre de Leon, J., Rehr, J. J., Zabinsky, S. I., & Albers, R. C. (1991) *Phys. Rev. B 44*, 4146−4156.
Nagamune, T., Kurata, H., Hirata, M., Honda, J., Koike, H., Ikeuchi, M., Inoue, Y., Hirta, A., & Endo, I. (1990) *Biochem. Biophys. Res. Commun. 168*, 437−442.
Nagamune, T., Honda, J., Kobayashi, Y., Sasabe, H., Endo, I., Ambe, F., Teratani, Y., & Hirata, A. (1992) *Hyperfine Interact. 71*, 1271−1274.
Nagasawa, T., Ryuno, K., & Yamada, H. (1986) *Biochem. Biophys. Res. Commun. 139*, 1305−1312.
Nagasawa, T., Takeuchi, K., & Yamada, Y. (1988) *Biochem. Biophys. Res. Commun. 155*, 1008−1016.
Nakajima, Y., Doi, T., Satoh, Y., Fujiwara, A., & Watanabe, I. (1987) *Chem. Lett.*, 1707−1770.
Nelson, M. J., Jin, H., Turner, I. M., Jr., Grove, G., Scarrow, R. C., Brennan, B. A., & Que, L., Jr. (1991) *J. Am. Chem. Soc. 113*, 7072−7073.
Nelson, M. J., Brennan, B. A., Chase, D. B., Cowling, R. A., Grove, G. N., & Scarrow, R. C. (1995) *Biochemistry 34*, 15219−15229.
Nishiyama, M., Horinouchi, S., Kobayashi, M., Nagasawa, T., Yamada, H., & Beppu, T. (1991) *J. Bacteriol. 173*, 2465−2472.
Noguchi, T., Honda, J., Nagamune, T., Sasabe, H., Inoue, Y., & Endo, I. (1995) *FEBS Lett. 358*, 9−12.
Que, L., Jr., Bobrik, M. A., Ibers, J. A., & Holm, R. H. (1974) *J. Am. Chem. Soc. 96*, 4168−4177.
Radonovich, L. J., Bloom, A., & Hoard, J. L. (1972) *J. Am. Chem. Soc. 94*, 2073−2078.
Randall, C. R., Shu, L., Chiou, Y.-M., Kagen, K. S., Ito, M., Kitajima, N., Lachicotte, R. J., Zang, Y., & Que, L., Jr. (1995) *Inorg. Chem. 34*, 1036−1039.
Raston, C. L., White, A. H., & Yandell, J. K. (1979) *Aust. J. Chem. 32*, 291−296.
Rehr, J. J., de Leon, J. M., Zabinsky, S. I., & Albers, R. C. (1991) *J. Am. Chem. Soc. 113*, 5135−5140.
Rehr, J. J., Albers, R. C., & Zabinsky, S. I. (1992) *Phys. Rev. Lett. 69*, 3397−3400.
Roe, A. L., Schneider, D. J., Mayer, R. J., Pyrz, J. W., Widom, J., & Que, L., Jr. (1984) *J. Am. Chem. Soc. 106*, 1676−1681.
Ryabova, N. A., Ponomarev, V. I., Atovmyan, L. O., Zelentsov, V. V., & Shipilov, V. I. (1978) *Koord. Khim. 4*, 119−126.
Ryabova, N. A., Ponomarev, V. I., Udel'nov, A. I., Zelentsov, V. V., & Kaftanat, V. N. (1979) *Zh. Strukt. Khim. 20*, 185−189.
Ryabova, N. A., Ponomarev, V. I., Zelentsov, V. V., Shipilov, V. I., & Atovmyan, L. O. (1981) *Zh. Strukt. Khim. 22* (2), 111−115.
Ryabova, N. A., Ponomarev, V. I., Zelentsov, V. V., & Atovmyan, L. O. (1982a) *Kristallografiya 27*, 81−91.
Ryabova, N. A., Ponomarev, V. I., Zelentsov, V. V., & Atovmyan, L. O. (1982b) *Kristallografiya 27*, 279−287.
Sato, T., Shiro, M., & Koyama, H. (1968) *J. Chem. Soc. B*, 989−994.
Sato, T., Tsukuda, Y., Shiro, M., & Koyama, H. (1969) *J. Chem. Soc. B*, 125−130.
Scarrow, R. C., Trimitsis, M. G., Buck, C. P., Grove, G. N., Cowling, R. A., & Nelson, M. J. (1994) *Biochemistry 33*, 15023−15035.
Scheidt, W. R., & Piciulo, P. L. (1976) *J. Am. Chem. Soc. 98*, 1913−1919.
Scheidt, W. R., Brinegar, A. C., Ferro, E. B., & Kirner, J. F. (1977) *J. Am. Chem. Soc. 99*, 7315−7322.
Scott, R. A. (1985) *Methods Enzymol. 117*, 414−459.
Seefeldt, L. C., Ryle, M. J., Lanzilotta, W. N., Scarrow, R. C., & Jensen, G. M. (1996) *J. Biol. Chem. 271*, 1551−1557.
Seel, F., Lehnert, R., Bill, E., & Trautwein, A. (1980) *Z. Naturforsch., B: Anorg. Chem., Org. Chem. 35*, 631−638.
Sellmann, D., Kunstmann, H., Moll, M., & Knoch, F. (1988) *Inorg. Chim. Acta 154*, 157−167.
Sellmann, D., Mahr, G., & Knoch, F. (1991) *Angew. Chem., Int. Ed. Engl. 30*, 1477−1479.
Shoner, S. C., Barnhart, D., & Kovacs, J. A. (1995) *Inorg. Chem. 34*, 4517−4518.
Sugiura, Y., Kuwahara, J., Nagasawa, T., & Yamada, H. (1987) *J. Am. Chem. Soc. 109*, 5848−5850.
Thorp, H. H. (1992) *Inorg. Chem. 31*, 1585−1588.
Zavodnik, V. E., Belsky, V. K., Voloshin, Y. Z., & Varzatskii, O. A. (1993) *J. Coord. Chem. 28*, 97−103.

BI960164L